JOURNAL OF GUIDANCE, CONTROL, AND DYNAMICS
Vol. 16, No. 6, November–December 1993

Optimal Periodic Control for Spacecraft Pointing and Attitude Determination

Mark E. Pittelkau*
Swales and Associates, Inc., Beltsville, Maryland 20705

A new approach to autonomous magnetic roll/yaw control of polar-orbiting, nadir-pointing momentum bias spacecraft is considered as the baseline attitude control system for the next Tiros series. It is shown that the roll/yaw dynamics with magnetic control are periodically time varying. An optimal periodic control law is then developed. The control design features a state estimator that estimates attitude, attitude rate, and environmental torque disturbances from Earth sensor and sun sensor measurements; no gyros are needed. The state estimator doubles as a dynamic attitude determination and prediction function. In addition to improved performance, the optimal controller allows a much smaller momentum bias than would otherwise be necessary. Simulation results are given.

I. Introduction

A MOMENTUM bias system is often considered for spacecraft attitude control because of potentially lower cost and weight and greater reliability than a zero momentum system. Magnetic roll/yaw control of momentum bias spacecraft such as ERBS, SAGE, and HCMM is traditionally based on the method of Stickler and Alfriend.[1] By their control law, the pitch magnetic moment d_y is given by

$$d_y = K_p B_x \delta_x + K_n \dot{B}_y \tag{1}$$

where B_x and B_y are measured roll and pitch components of the local geomagnetic field, δ_x is the roll attitude as measured by an Earth sensor, and K_p and K_n are the precession gain and the nutation gain. For the most part, this law provides damping feedback whereas the attitude response to disturbances is largely determined by the momentum bias. For roll and yaw torque disturbances (τ_{dx} and τ_{dz}) at frequencies from zero up to the orbital frequency ω_o, the roll and yaw attitude errors (δ_x and δ_z, hereafter simply called attitude) are determined by the rule-of-thumb design equation

$$\frac{\delta_x}{\tau_{dx}} = \frac{\delta_z}{\tau_{dz}} = -\frac{1}{h_y \omega_o} \tag{2}$$

where h_y is the wheel momentum. Given limits on the roll and yaw attitude and estimates of the roll and yaw torque disturbances, one often finds that the required momentum bias is exceedingly large forcing the consideration of a zero momentum system. For example, if attitude is to be kept within 0.002 mrad and the disturbance at low frequency is 0.004 N, then for $\omega_o = 0.001$ rad/s we require $h_y = 2000$ Nms, which is large by any standard.

The two basic approaches to attitude estimation (determination) involve either a kinematic model of attitude or a dynamic model.[2,3] The dynamic model approach requires a model of attitude dynamics to propagate an estimated attitude state vector and attitude measurements to update the estimated state. The kinematic model utilizes three-axis gyro measurements to propagate an estimated quaternion state vector and occasional attitude measurements to update the estimated state.[2] The state vector is augmented with gyro bias states that are also estimated. A serious drawback to the kinematic approach is the large cost and inherent unreliability of the gyro package.

In Ref. 2 it is stated that the dynamic model approach is limited by uncertainties in the model due to external torques and internal momentum of rotating or rastering instruments. Since the momentum of the instruments can be internally compensated or otherwise limited by design, and since the frequency of this momentum is usually on the order of 0.1 to 1 Hz, internal momentum may not be a serious problem. By augmenting the dynamic model of spacecraft motion with a model of the external torque disturbance, estimates of attitude, attitude rate, and disturbance torques can be obtained with only Earth sensor and sun sensor measurements, as will be shown in this paper. These estimates are predicted during periods of sun occlusion and when Earth sensor measurements are not utilized because of increased measurement error due to radiance gradients or sun or moon interference.

Dynamic propagation of attitude was considered for Nimbus-6 by processing telemetered data on the ground, but this attempt suffered from a variety of difficulties.[4,5] More recently, dynamic propagation of attitude was considered for GOES-Next[5] as an alternative to kinematic propagation so that the gyros can be turned off during routine operations to extend their life span. In Ref. 5, attitude, attitude rate, and environmental torque disturbances are estimated from measurements of roll/yaw attitude and wheel speed.

The orbital and body reference frames are defined as follows. The orbital reference frame is defined such that its z axis points to the center of the Earth. Its y axis is parallel to a vector normal to the plane of the orbit such that the inertial angular rate of the spacecraft in its orbit is negative along this axis. The x axis is perpendicular to the other two axes and nominally in the direction of the velocity vector to complete a right-handed frame. The zero position of the orbital reference frame is at the equator, i.e., the ascending node for an afternoon polar orbit and the descending node for a morning polar orbit. For zero attitude error, the attitude control coordinate frame—or body frame—is aligned with the orbital reference frame.

Throughout this paper, x and z with various subscripts are used to denote state vectors or outputs. They are also used as subscripts to denote x and z coordinate axes.

II. Optimal Magnetic Control

A deficiency of the Stickler and Alfriend control law given by Eq. (1) is that it is nondynamic and nonoptimal. (A dynamic controller is one in which the control is a frequency-dependent function of the measurements, i.e., the controller has

Received May 11, 1992; revision received Dec. 14, 1992; accepted for publication Jan. 14, 1993.

*Control Systems Engineer, Controls and Dynamics Group, 5050 Powder Mill Road. Member AIAA.

states governed by a differential or difference equation of a certain order. A nondynamic, or memoryless, controller is one in which the control is instantaneously dependent on the measurements but not on past measurements.) Hence the limit of performance of magnetic control has not yet been realized. A periodic linear quadratic optimal control approach to autonomous magnetic control of momentum bias spacecraft is being considered as the baseline for the next series of Tiros spacecraft (designated NOAA O, P, and Q), the first of which is to be launched in 2001.[6] This optimal design is based on the periodic nature of the roll/yaw dynamics with magnetic actuators. Consider the dipole model of the Earth's magnetic field in the orbital reference frame

$$ {}^{O}\boldsymbol{B} = b_m \begin{pmatrix} \cos\lambda \\ 0 \\ 2\sin\lambda \end{pmatrix} = b_m \begin{pmatrix} \cos\omega_o t \\ 0 \\ 2\sin\omega_o t \end{pmatrix} \tag{3} $$

where $\lambda = \omega_o t$ is the orbital latitude and $b_m = \mu_m/(r_e + r_a)^3$ is the magnetic field strength at the orbital altitude r_a relative to the mean radius r_e of the Earth. At $r_a = 824$ km, $b_m = 2.13(10^{-5})$ T.

Let ${}^{B}\boldsymbol{D} = (d_x\ d_y\ d_z)^T$ denote the magnetic moment produced by three orthogonal magnetic torquer bars aligned with the body reference frame. Since attitude will be regulated to nearly zero, any slight misalignment between the torquer bars and the orbital reference frame is neglected, i.e., ${}^{B}\boldsymbol{B} \simeq {}^{O}\boldsymbol{B}$. The interaction of the magnetic moment ${}^{B}\boldsymbol{D}$ (measured in joules/tesla = Am^2) and the magnetic field ${}^{B}\boldsymbol{B}$ of the Earth generates a control torque

$$ {}^{B}\tau_c = {}^{B}\boldsymbol{D} \times {}^{B}\boldsymbol{B} $$

$$ {}^{B}\tau_c = \begin{pmatrix} \tau_{cx} \\ \tau_{cy} \\ \tau_{cz} \end{pmatrix} = b_m \begin{pmatrix} 2d_y \sin\omega_o t \\ d_z \cos\omega_o t - 2d_x \sin\omega_o t \\ -d_y \cos\omega_o t \end{pmatrix} \tag{4} $$

Since the linearized pitch dynamics are decoupled from the roll/yaw dynamics, the pitch dynamics are made time invariant by computing the roll and yaw torquer bar moments as $d_x = -d\sin\omega_o t$ and $d_z = 2d\cos\omega_o t$ to get the time-invariant relation $\tau_{cy} = 2b_m d$, where d is the output of the pitch attitude controller described in Refs. 6 and 7. No such transformation is possible with the roll/yaw control moment since the first and third elements of Eq. (4) both depend linearly on the single control variable d_y. This dependency is periodically time varying. Since the roll and yaw control torques at each latitude cannot be arbitrary in direction, the control effort should be optimized.

The linearized dynamics are given by[6,8]

$$ I_x\ddot{\delta}_x - [h_y\omega_o - 4\omega_o^2(I_y - I_z)]\delta_x - [h_y + \omega_o(I_x - I_y + I_z)]\dot{\delta}_z = \tau_{cx} + \tau_{dx} \tag{5} $$

$$ I_y\ddot{\delta}_y + 3\omega_o^2(I_x - I_z)\delta_y = \tau_{cy} + \tau_{dy} - \dot{h}_y \tag{6} $$

$$ I_z\ddot{\delta}_z - [h_y\omega_o - \omega_o^2(I_y - I_x)]\delta_z + [h_y + \omega_o(I_x - I_y + I_z)]\dot{\delta}_x = \tau_{cz} + \tau_{dz} \tag{7} $$

where $I_x = 5764$, $I_y = 6147$, $I_z = 10{,}821$ kg-m^2, $h_y = -420$ Nms, and $\omega_o = 0.00103448$ rad/s. Substituting Eq. (4) for τ_{cx} and τ_{cz}, Eqs. (5) and (7) are written in a normalized state space form as

$$ \begin{bmatrix} \dot{\delta}_x \\ \dot{\delta}_z \\ \ddot{\delta}_x \\ \ddot{\delta}_z \end{bmatrix} = \begin{bmatrix} 0 & 0 & \omega_n & 0 \\ 0 & 0 & 0 & \omega_n \\ a_{31} & 0 & 0 & a_{34} \\ 0 & a_{42} & a_{43} & 0 \end{bmatrix} \begin{bmatrix} \delta_x \\ \delta_z \\ \dot{\delta}_x \\ \dot{\delta}_z \end{bmatrix} + \begin{bmatrix} 0 \\ 0 \\ \dfrac{2b_m \sin\omega_o t}{\omega_n I_x} \\ \dfrac{-b_m \cos\omega_o t}{\omega_n I_z} \end{bmatrix} d_y + \begin{bmatrix} 0 & 0 \\ 0 & 0 \\ 1/\omega_n I_x & 0 \\ 0 & 1/\omega_n I_z \end{bmatrix} \begin{bmatrix} \tau_{dx} \\ \tau_{dz} \end{bmatrix} \tag{8} $$

where

$$ a_{31} = [h_y\omega_o - 4\omega_o^2(I_y - I_z)]/\omega_n I_x \tag{9} $$

$$ a_{34} = [h_y + \omega_o(I_x - I_y + I_z)]/I_x \tag{10} $$

$$ a_{42} = [h_y\omega_o - \omega_o^2(I_y - I_x)]/\omega_n I_z \tag{11} $$

$$ a_{43} = -[h_y + \omega_o(I_x - I_y + I_z)]/I_z \tag{12} $$

Observe that the attitude rates are scaled by the nutation frequency $\omega_n = -h_y/\sqrt{I_x I_z}$ so that $\dot{\delta}_x = \omega_n\dot{\tilde{\delta}}_x$ and $\dot{\delta}_z = \omega_n\dot{\tilde{\delta}}_z$. This normalized form is chosen partly to improve the numerical properties of the controller design and analysis. For the case where $I_x \simeq I_z$, the normalized from has the advantage that $a_{31} \simeq \omega_o$, $a_{34} \simeq \omega_o + \omega_n$, $a_{42} \simeq \omega_o$, and $a_{43} \simeq -(\omega_o + \omega_n)$ so that state and input transition matrices are easily obtained for a discrete-time implementation.[5] Unfortunately, $I_x \simeq I_z$ is not the case here.

In shorthand notation, Eq. (8) is written

$$ \dot{x}_p = A_p x_p + B_p(t)d_y + [B_x \quad B_z]\begin{bmatrix} \tau_{dx} \\ \tau_{dz} \end{bmatrix} \tag{13} $$

The dependence of B_p on time is shown explicitly in Eq. (13). Equations (8) and (13) are periodic with period $\rho = 2\pi/\omega_o$ since $B_p(t) = B_p(t + \rho)$. Measured states are given by

$$ \delta_m = \begin{bmatrix} \delta_{x,m} \\ \delta_{z,m} \end{bmatrix} = C_p x_p + \nu \tag{14} $$

where $\delta_{x,m}$ is the roll angle measured by an Earth sensor, $\delta_{z,m}$ the yaw angle measured by a sun sensor, ν the measurement error, and $C_p = [I_{2\times 2} \quad 0_{2\times 2}]$.

Disturbance Modeling

Analytical expressions were derived for the gravity gradient, dynamic, and other environmental torques as a function of solar array rotation angle. These expressions show that the most significant disturbances are sinusoids at frequencies 0 and ω_o about the roll axis and at 0, ω_o, and $2\omega_o$ about the yaw axis. Disturbance rejection is achieved by augmenting Eq. (13) with models of these disturbances in a linear quadratic control design. Since the disturbance states are uncontrollable, stable models are required for the computation of state feedback gains. Stable models for disturbances at 0, ω_o, and $2\omega_o$ are given by the proportional-integral and unity gain bandpass functions

$$ D_0(s) = 1/(s + \epsilon) + K_o \tag{15} $$

$$ D_1(s) = \frac{2\zeta_o\omega_o s}{s^2 + 2\zeta_o\omega_o s + \omega_o^2} \tag{16} $$

$$ D_2(s) = \frac{4\zeta_o\omega_o s}{s^2 + 4\zeta_o\omega_o s + 4\omega_o^2} \tag{17} $$

where $\epsilon = 10^{-6}$ and $\zeta_o > 0$ make the models stable and K_o is chosen to place a closed-loop pole at $-1/K_o$. The state equation for the estimator can be implemented with $\epsilon = 0$ and $\zeta_o = 0$. The damping ζ_o is usually on the order of 0.01 to 0.001, but should be large enough so that uncertainty in ω_o due to orbit decay and other effects lies within the bandpass. The 3-dB bandwidth of the bandpass filters is $2\zeta_o\omega_o$ for Eq. (16) and $4\zeta_o\omega_o$ for Eq. (17). Then for a 1% uncertainty in ω_o, one should set $\zeta_o = 0.005$. Note, however, that the estimated disturbances may converge slowly and will converge with greater residual error if ζ_o is much larger than 0.01, and this limits the uncertainty that can be accepted. The estimator is easily tuned on orbit, if necessary.

Convenient state space representations for Eqs. (15–17) driven by white noise processes η_0, η_1, and η_2 are given by

$$\dot{x}_0 = -\epsilon x_0 + \eta_0$$
$$z_0 = x_0 + K_o\eta_0 \tag{18}$$

$$\begin{bmatrix}\dot{x}_{11}\\ \dot{x}_{12}\end{bmatrix} = \begin{bmatrix}\sigma & \omega_d\\ -\omega_d & \sigma\end{bmatrix}\begin{bmatrix}x_{11}\\ x_{12}\end{bmatrix} + \begin{bmatrix}-2\sigma\\ -2\sigma^2/\omega_d\end{bmatrix}\eta_1$$
$$z_1 = [1 \quad 0]\begin{bmatrix}x_{11}\\ x_{12}\end{bmatrix} \tag{19}$$

$$\begin{bmatrix}\dot{x}_{21}\\ \dot{x}_{22}\end{bmatrix} = 2\begin{bmatrix}\sigma & \omega_d\\ -\omega_d & \sigma\end{bmatrix}\begin{bmatrix}x_{21}\\ x_{22}\end{bmatrix} + 2\begin{bmatrix}-2\sigma\\ -2\sigma^2/\omega_d\end{bmatrix}\eta_2$$
$$z_2 = [1 \quad 0]\begin{bmatrix}x_{21}\\ x_{22}\end{bmatrix} \tag{20}$$

where $\sigma = -\zeta_o\omega_o$ and $\omega_d = \omega_o\sqrt{1-\zeta_o^2}$. This representation was chosen because it is numerically balanced and leads to a simple form of the state transition matrix. In shorthand notation, Eqs. (18–20) are written

$$\dot{x}_0 = A_0x_0 + B_0\eta_0 \qquad z_0 = C_0x_0 + K_o\eta_0 \tag{21}$$

$$\dot{x}_1 = A_1x_1 + B_1\eta_1 \qquad z_1 = C_1x_1 \tag{22}$$

$$\dot{x}_2 = A_2x_2 + B_2\eta_2 \qquad z_2 = C_2x_2 \tag{23}$$

A torque disturbance τ_d is thus obtained by adding its components, i.e., $\tau_d = z_0 + z_1 + z_2$.

Augmented Plant Model

In Ref. 5 the roll and yaw disturbance torques were assumed to be 90 deg out of phase and of equal amplitude at a single frequency ω_o, so a single disturbance model was used. The states in Eq. (19) represent sinusoids that are 90 deg out of phase but with equal amplitudes, and similarly in Eq. (20). The sinusoidal torque disturbances in roll and yaw, however, are only approximately 90 deg out of phase and are of different amplitude. As a result, independent models are required to represent roll and yaw disturbances even though their frequencies are the same.

The plant state and output equations (13) and (14) are augmented with the disturbances models (21), (22), and (23). [This plant augmentation with an external disturbance model (i.e., the "external model principle") is dual to the internal model principle utilized in Ref. 10.] The states of the disturbance models are further subscripted with x and z to denote their respective coordinate directions. Since there is no disturbance in roll at $2\omega_o$, the corresponding disturbance model (23) is omitted from the roll equation. The augmented system is thus represented by

$$\begin{bmatrix}\dot{x}_p\\ \dot{x}_{0x}\\ \dot{x}_{1x}\\ \dot{x}_{0z}\\ \dot{x}_{1z}\\ \dot{x}_{2z}\end{bmatrix} = \begin{bmatrix}A_p & B_xC_0 & B_xC_1 & B_zC_0 & B_zC_1 & B_zC_2\\ 0 & A_0 & 0 & 0 & 0 & 0\\ 0 & 0 & A_1 & 0 & 0 & 0\\ 0 & 0 & 0 & A_0 & 0 & 0\\ 0 & 0 & 0 & 0 & A_1 & 0\\ 0 & 0 & 0 & 0 & 0 & A_2\end{bmatrix}\begin{bmatrix}x_p\\ x_{0x}\\ x_{1x}\\ x_{0z}\\ x_{1z}\\ x_{2z}\end{bmatrix}$$
$$+ \begin{bmatrix}B_p(t)\\ 0\\ 0\\ 0\\ 0\\ 0\end{bmatrix}d_y + \begin{bmatrix}B_xK_o & 0 & B_zK_o & 0 & 0\\ B_0 & 0 & 0 & 0 & 0\\ 0 & B_1 & 0 & 0 & 0\\ 0 & 0 & B_0 & 0 & 0\\ 0 & 0 & 0 & B_1 & 0\\ 0 & 0 & 0 & 0 & B_2\end{bmatrix}\begin{bmatrix}\eta_{0x}\\ \eta_{1x}\\ \eta_{0z}\\ \eta_{1z}\\ \eta_{2z}\end{bmatrix} \tag{24}$$

$$x_p = [I_{4\times4} \quad 0 \quad 0 \quad 0 \quad 0 \quad 0]x \tag{25}$$

$$\delta_m = [C_p \quad 0 \quad 0 \quad 0 \quad 0 \quad 0]x + \nu \tag{26}$$

where $x^T = (x_p^T \; x_{0x} \; x_{1x}^T \; x_{0z} \; x_{1z}^T \; x_{2z}^T)$ is the state vector in Eq. (24) and is of dimension 12. The state and output equations (24–26) are now written as

$$\dot{x} = Ax + B(t)d_y + H\eta \tag{27}$$

$$x_p = Cx \tag{28}$$

$$\delta_{x,m} = C_mx + \nu \tag{29}$$

The time dependence of the input matrix $B(t)$ is shown explicitly in Eqs. (24) and (27), whereas the time dependence of the state and input variables is suppressed. The matrices A and H are constant. The process noise η has stationary statistics with mean zero and covariance $Q_\eta = \mathcal{E}\{\eta\eta^T\} = \text{diag}(q_1, \ldots, q_7)$. These statistics do not need to reflect the actual statistics of the noise process and will be used to tune a state estimator for good performance and to achieve a certain gain and phase margin.

State Feedback Design

The quadratic performance index is given by

$$J = \int_0^T (u^TR_cu + x^TQ_cx)\,dt \tag{30}$$

where the control $u = d_y$, $R_c > 0$ is a control weighting matrix, and $Q_c \geq 0$ is a state weighting matrix. By choosing $Q_c = C^TWC$, where W is a diagonal weighting matrix, the performance index (30) gives a tradeoff between the control u $(= d_y)$ and the state $x_p = Cx$. Minimizing Eq. (30) subject to Eqs. (27) and (28) results in the Riccati differential equation[9,11]

$$\dot{P}_c = -P_cA - A^TP_c + P_cB(t)R_c^{-1}B^T(t)P_c - Q_c \tag{31}$$

where $P_c = P_c(t,T) > 0$ with boundary condition $P_c(T,T) = 0$. By solving the Riccati equation backward in time (via numerical integration) and letting the time horizon $T \to \infty$ [i.e., $P_c(t,T) \to P_c(t)$], the matrix P_c converges to a periodic function $P_c(t+\rho) = P_c(t)$ with period $\rho = 2\pi/\omega_o$ since $B(t+\rho) = B(t)$ is periodic with period ρ (see Refs. 12–15). The minimizing (optimal) control is

$$d_y(t) = u(t) = K_c(t)x(t) \tag{32}$$

where the state feedback gain matrix given by

$$K_c(t) = -R_c^{-1}B^T(t)P_c(t) \tag{33}$$

ensures that the periodic closed-loop system $\dot{x} = [A + B(t)K_c(t)]x$ is uniformly asymptotically stable.[15] Note that the state feedback gain vector $K_c(t) = K_c(t + \rho)$ is also periodic with period ρ.

The LSODE numerical integration package[16] was used to integrate the Riccati differential equation (31) (which is a stiff equation) backward in time from $t = 2\rho$ to 0. The 12 state feedback gains (elements of K_c) were computed with $R_c = 10^{-11}$ and $W = \text{diag}(2,1,0,0)$. The position and rate gains (Many of these gains strongly resemble the solution to the famous Van der Pol equation, but reversed in time.) are plotted in Figs. 1 and 2 for $T = 2\rho$, i.e., two orbits. The time scale in the plotted results is normalized by the orbital period, i.e., t/ρ. Note that the gains settle down to a periodic steady state after about one orbit. The gains computed over the last orbit are stored in a file at 5.82-s intervals (1000 samples per orbit). This gain schedule will be stored in the on-orbit attitude control processor but at a lower density. Note that gains for only one-half of the orbit need to be stored since they are odd functions. Linear interpolation is used to compute gains at times between samples and is sufficient at 1000 samples per orbit, as simulation results indicate, but spline interpolation may be required for low density storage.

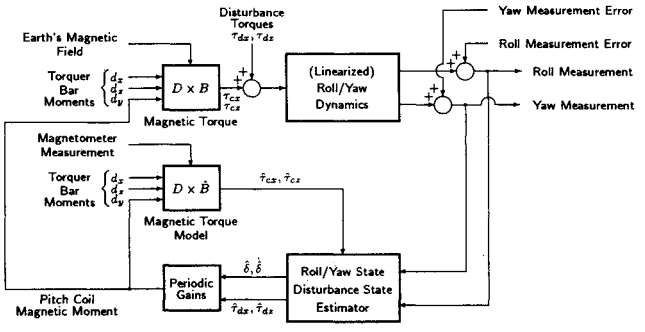

Fig. 1 Roll and yaw attitude gains.

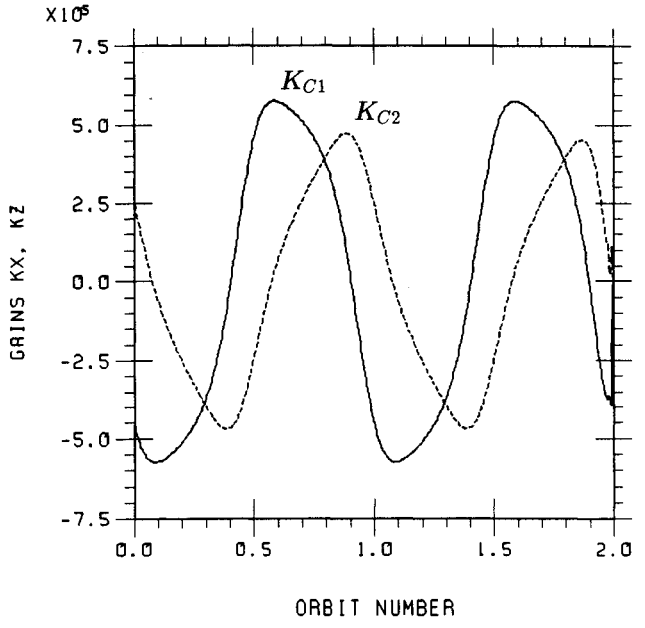

Fig. 2 Roll and yaw attitude rate gains.

State Estimator Design

Since roll and yaw attitude are the only measured states, the remaining states—roll and yaw attitude rates and the disturbance torques—must be estimated. Roll and yaw attitude is also estimated to provide smooth attitude data. These states are predicted during periods of sun occlusion and where Earth sensor measurements are not utilized because of increased measurement error due to radiance gradients or sun or moon interference. A state estimator for the system represented by Eqs. (27) and (29) is given by

$$\dot{\hat{x}} = A\hat{x} + B(t)d_y + K_e(\delta_m - C_m\hat{x}) \tag{34}$$

where $\hat{x}$ is the estimated state vector. Given the solution P_e to the algebraic Riccati equation

$$0 = P_eA^T + AP_e - P_eC_m^TR_e^{-1}C_mP_e + Q_e \tag{35}$$

the Kalman-Bucy gain K_e is computed by

$$K_e = -P_eC_m^TR_e^{-1} \tag{36}$$

In this case, $R_e > 0$ is a scalar and $Q_e = HQ_\eta H^T$, where the diagonal matrix $Q_\eta = \mathcal{E}\{\eta\eta^T\}$ was defined previously and H is defined by Eqs. (24) and (27). For a statistically optimal design, one would choose $R_e = \mathcal{E}\{v^2\}$, but this is unnecessarily restrictive in control system design. The structure of the matrix Q_e is chosen so that the loop transfer properties of the state feedback controller (namely, its inherently good gain and phase margin) are recovered as R_e is decreased. Equations (35) and (36) were evaluated using MATLAB. The estimator gain was computed with $\zeta_o = 0.001$, $K_o = 1$, $R_e = \text{diag}(10^{-13}, 10^{-13})$, and

$$Q_\eta = \text{diag}[0,\ 0,\ 0.05,\ 10^5,\ 0.05,\ 10^5,\ 2(10^4)] \tag{37}$$

It was found during the course of development of the optimal controller that, given only roll measurements, disturbances in roll and yaw at the orbital frequency could not be estimated without error, although the rms value of the roll and yaw torque estimates matched the actual rms value. The matrix P_e from Eq. (35) showed a large covariance associated with yaw when only roll measurements are taken. The resulting attitude estimate error was zero in roll and varied as $-1.5 + 4 \sin \omega_o t$ mrad in yaw. Control accuracy was not significantly improved with the improved yaw attitude estimation.

Although practical theories and results for linear quadratic Gaussan (LQG) control of periodic systems are sparsely available in the literature, theories such as in Ref. 17 may prove to be useful. Analysis of stability, robustness, and frequency response are key areas requiring further research. Despite the paucity of such results, LQG control design for periodic systems has produced useful results as shown in the next section.

III. Analysis of Results

Torque disturbances due to gravity gradient, the dynamic effect of the orbital pitch rate, aerodynamic force, solar pressure, and orbit precession were derived analytically and are summarized as

$$\tau_{dx} = 4.3(10^{-4}) - 6.1(10^{-3})\cos \omega_o t - 8.4(10^{-5})\sin \omega_o t \tag{38}$$

$$\tau_{dy} = 2.0(10^{-4}) - 4.7(10^{-4})\cos \omega_o t - 1.2(10^{-4})\sin \omega_o t - 2.7(10^{-4})\sin 2\omega_o t + 1.1(10^{-4})\cos 3\omega_o t \tag{39}$$

$$\tau_{dz} = -5.1(10^{-4}) + 2.4(10^{-3})\sin \omega_o t + 9.2(10^{-4})\cos 2\omega_o t \tag{40}$$

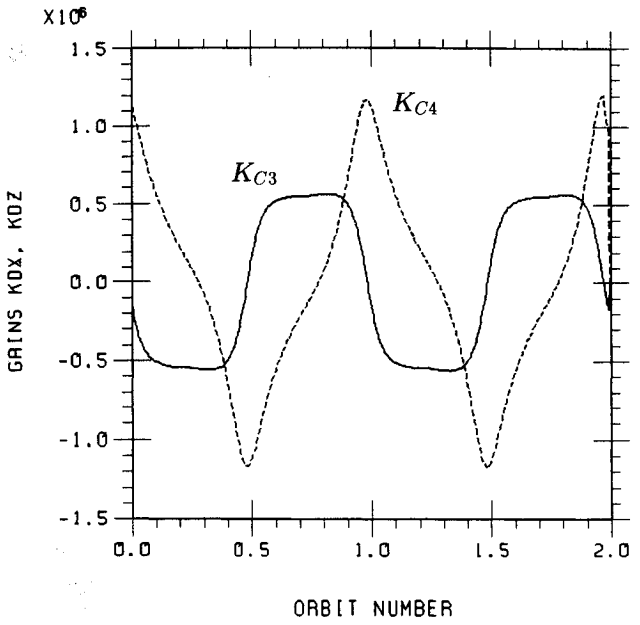

Fig. 3 Roll/yaw control system block diagram.

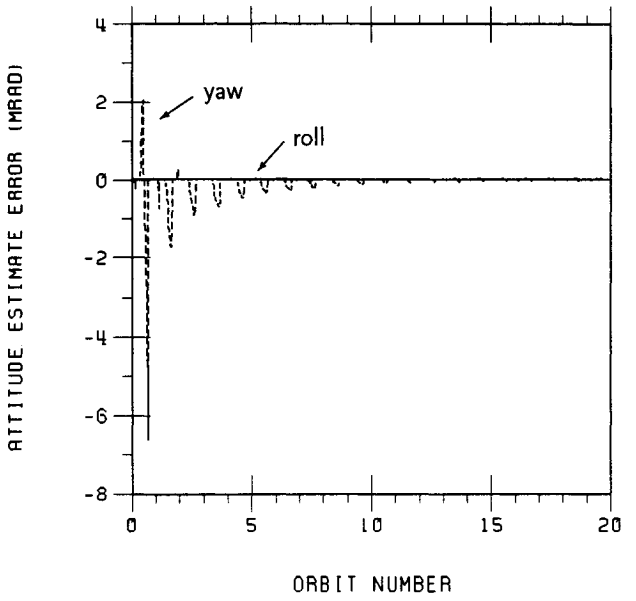

Fig. 5 Roll and yaw attitude estimate error.

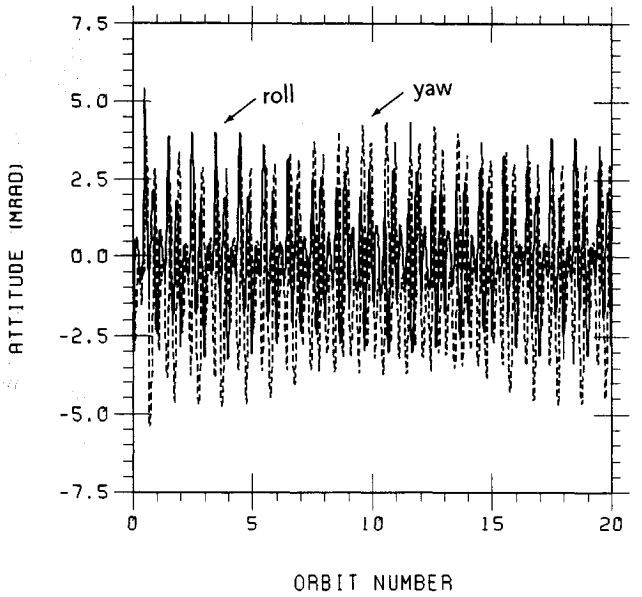

Fig. 4 Roll and yaw attitude.

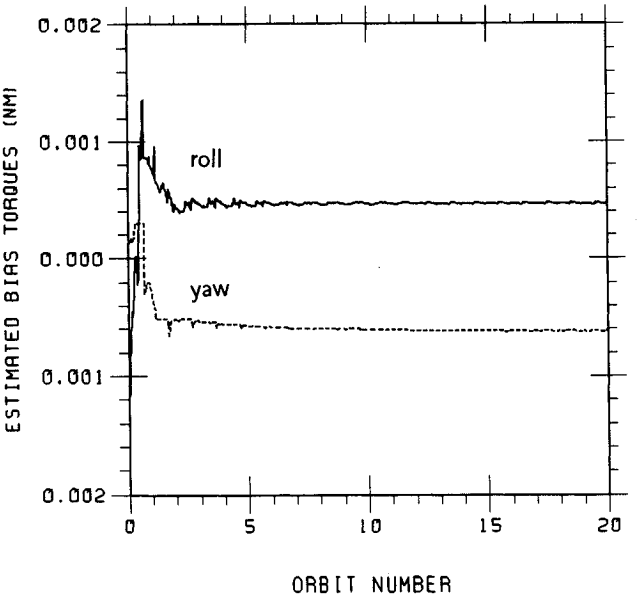

Fig. 6 Estimated bias disturbance torques.

These expressions are with respect to the ascending node of an afternoon orbit. Sun angle variations up to ± 23 deg, which are not included in these expressions but arise from solar array tracking of the sun, have little effect on simulation results. Occlusion of the sun between 117.7- and 242.3-deg orbital latitude, ± 23 deg, which results in reduced yaw observation, was simulated.

The magnetic dipole equation (3) is used for design only. In the truth model used for simulation, the dipole field of the Earth is tilted at $\epsilon = 11.4$ deg from north and rotates about the north axis at the rotation rate ω_e of the Earth. The components of ${}^{B}\boldsymbol{B}$ are given by

$$b_x = b_m\{a_1\cos\omega_o t - b_1\cos[(\omega_o - \omega_e)t - \alpha] + b_2\cos[(\omega_o + \omega_e)t + \alpha)]\} \tag{41}$$

$$b_y = b_m[-a_2 - a_3\cos(\omega_e t + \alpha)] \tag{42}$$

$$b_z = b_m\{2a_1\sin\omega_o t - 2b_1\sin[(\omega_o - \omega_e)t - \alpha] + 2b_2\sin[(\omega_o + \omega_e)t + \alpha]\} \tag{43}$$

where α is a phase angle,

$$a_1 = \sin i\cos\epsilon \qquad b_1 = \tfrac{1}{2}(1 + \cos i)\sin\epsilon$$

$$a_2 = \cos i\cos\epsilon \qquad b_2 = \tfrac{1}{2}(1 - \cos i)\sin\epsilon$$

$$a_3 = \sin i\sin\epsilon$$

and where $i = 98.6$ deg is the orbital inclination in the present case. Equations (41-43) are used as a truth model in a simulation program. Higher order harmonics of the Earth's magnetic field are not modeled. These harmonic components, which are small in magnitude, create small torque disturbances, some of which are readily rejected by the controller since they are at frequencies 0, ω_o, and $2\omega_o$.

To improve the accuracy and robustness of the state estimator, the components of $B(t)d_y$ in Eq. (34) representing the

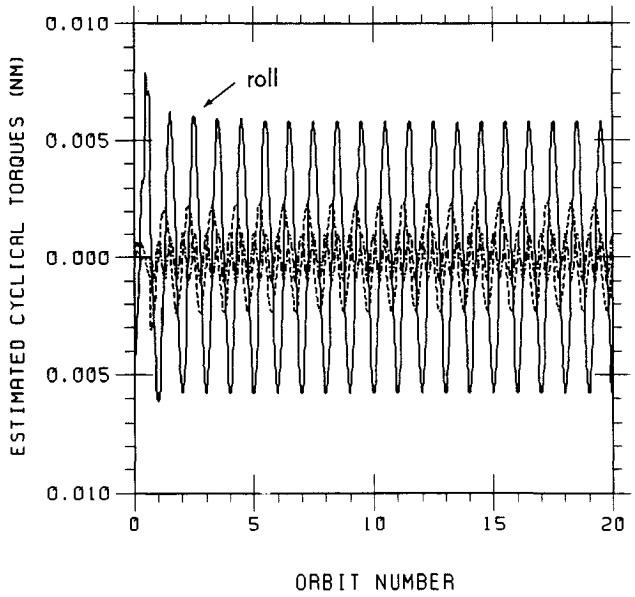

Fig. 7 Estimated cyclical disturbance torques.

control torque input to the plant are replaced by τ_{cx} and τ_{cz} from

$$ {}^{B}\boldsymbol{D} \times {}^{B}\boldsymbol{B}_m = \begin{pmatrix} \hat{\tau}_{cx} \\ \hat{\tau}_{cy} \\ \hat{\tau}_{cz} \end{pmatrix} = \begin{pmatrix} d_y b_z - d_z b_y \\ d_z b_x - d_x b_z \\ d_x b_y - d_y b_x \end{pmatrix} \tag{44} $$

where ${}^{B}\boldsymbol{B}_m$ is the Earth's magnetic field vector measured by three orthogonal fluxgate magnetometers. The block diagram of the system in Fig. 3 shows that the control torques $\hat{\tau}_{cx}$ and $\hat{\tau}_{cz}$ are input to the estimator, whereas the actual torque ${}^{B}\boldsymbol{D} \times {}^{B}\boldsymbol{B}$ produced by the magnetic field of the Earth is summed with the disturbance torque and input to the spacecraft. As indicated in the figure, linearized dynamics are used to model the spacecraft. Although a full Euler model may seem preferable, the linearized model is sufficient since attitude and attitude rate is small.

Because of the dipole tilt, $b_y \neq 0$, so the magnetic pitch control moments d_x and d_y couple into roll and yaw as a torque disturbance. Since $d_x = -d\sin\,\omega_o t$ and $d_z = 2d\cos\,\omega_o t$, the pitch control coupling disturbance torque in roll and yaw is

$$ -d_z b_y = 2b_m d[a_2 + a_3\cos(\omega_e t + \alpha)]\cos\,\omega_o t \tag{45} $$

$$ d_x b_y = b_m d[a_2 + a_3\cos(\omega_e t + \alpha)]\sin\,\omega_o t \tag{46} $$

As the pitch control moment d is proportional to the pitch disturbance torque by virtue of the pitch controller design,[6,7] the pitch control coupling disturbances are at frequencies 0, ω_o, $2\omega_o$, $3\omega_o$, and $4\omega_o$.

Since b_x and b_z vary according to Eqs. (41) and (43), the loop gains through roll, pitch, and yaw vary from $+7\%$ to -13%. Higher order field harmonics have not yet been examined. Magnetic coupling from the torquer bars into the magnetometers can be trimmed by placing small magnetic coils in series with the torquer bars near the magnetometer to buck the torquer bar moment. Magnetometer bias is not considered in the simulation program. Residual magnetic dipole of the spacecraft is hard to quantify and is also not considered.

Simulation results are shown in Figs. 4–7. No sensor noise or other systematic measurement error was simulated. The roll and yaw attitude of the spacecraft in Fig. 4 varies with a peak amplitude of ± 4 mrad after the initial transient subsides. (Sun occlusion had little bearing on this.) The variation in peak amplitude is due to Earth's rotation as predicted by Eqs. (41–43) and the analysis that follows. Figure 5 shows that without sensor noise or other systematic measurement error, the roll attitude estimate error is zero and the yaw attitude estimate error asymptotically approaches zero. The periodic divergence from zero is due to occlusion of the sun, where no yaw information is available. Figures 6 and 7 show that the bias and cyclical torque disturbances are estimated quite well in just a few orbits' time. (The transient due to zero initial states of the filter can be largely eliminated in on-orbit operation by initializing the disturbance state estimates with nonzero a priori estimates.) The magnetic control moment in the pitch torquer bar (not shown) is cyclical with a peak amplitude of ± 300 Am^2; the saturation limit of ± 500 Am^2 is never reached.

IV. Conclusion

A periodic linear quadratic Gaussian control law was developed for autonomous magnetic control of polar-orbiting, nadir-pointing momentum bias spacecraft. The control design uses state estimate feedback where the estimated states are attitude, attitude rate, bias torque disturbances, and torque disturbances at ω_o and $2\omega_o$; the bias momentum is relatively small, and no gyros are required. By comparison, the now classical magnetic control law is not optimal in any sense, does not utilize dynamic compensation, and requires a relatively large momentum bias. Furthermore, the roll attitude gain must be set to zero over a large portion of the orbit to prevent instability.

Simulation results of the optimal periodic controller show that roll and yaw attitude can be regulated to a small value despite large torque disturbances and a relatively small momentum wheel. Furthermore, attitude, attitude rate, and the torque disturbances are estimated quite well by processing roll and yaw measurements from an Earth sensor and a sun sensor. The state estimator doubles as a dynamic attitude determination function without the need for yaw gyro data.

Acknowledgments

The work generated here was performed under NASA contract NAS 5-30375. The author thanks the reviewers for their comments; they greatly improved the clarity of this article.

References

[1]Stickler, A. C., and Alfriend, K. T., "Elementary Magnetic Attitude Control System," *Journal of Spacecraft and Rockets,* Vol. 13, No. 5, 1976, pp. 282–287.

[2]Lefferts, E. J., Markley, F. L., and Shuster, M. D., "Kalman Filtering for Spacecraft Attitude Estimation," *Journal of Guidance, Control, and Dynamics,* Vol. 5, No. 5, 1982, pp. 417–429.

[3]Murrell, J. W., "Precision Attitude Determination for Multimission Spacecraft," AIAA Paper 78-1248, 1978.

[4]Lefferts, E. J., and Markley, F. L., "Dynamic Modeling for Attitude Determination," AIAA Paper 76-1910, Aug. 1976.

[5]Markley, F. L., Seidewitz, E., Chu, D., and Rowe, J. N., "GOES Dynamic Propagation of Attitude," *Flight Mechanics and Estimation Theory Symposium,* NASA CP 3011, May 1988, pp. 430–455.

[6]Anon., "NOAA O, P, Q Phase-A Study Final Report," Vol. II, National Technical Information Service, NTIS No. PB92150226, Jan. 1992.

[7]Pittelkau, M. E., "Frequency Weighted LQG Control of Spacecraft Attitude," *1st IEEE Conference on Control Applications,* Vol. 1, IEEE, New York, Sept. 1992, pp. 336–341.

[8]Wertz, J. R. (ed.), *Spacecraft Attitude Determination and Control,* D. Reidel, Boston, MA, 1980.

[9]Anderson, B. D. O., and Moore, J. B., *Optimal Control, Linear Quadratic Methods,* Prentice-Hall, Englewood Cliffs, NJ, 1990.

[10]Wie, B., and Gonzalez, M., "Control Synthesis for Flexible Space Structures Excited by Persistent Disturbances," *Journal of Guidance, Control, and Dynamics,* Vol. 15, No. 1, 1992, pp. 73–80.

[11]Choi, C. H., and Laub, A. J., "Efficient Matrix-Valued Algorithms for Solving Stiff Riccati Differential Equations," *IEEE Transactions Automatic Control,* Vol. 35, No. 7, 1990, pp. 770–776.

[12]Kano H., and Nishimura, T., "Controllability, Stabilizability,

and Matrix Riccati Equations for Periodic Systems," *IEEE Transactions on Automatic Control,* Vol. AC-30, No. 11, 1985, pp. 1129–1131.

[13]Hernández, V., and Jódar, L., "Boundary Problems and Periodic Riccati Equations," *IEEE Transactions on Automatic Control,* Vol. AC-30, No. 11, 1985, pp. 1131–1133.

[14]Bittani, S., Bolzern, P., Colaneri, P., and Guardabassi, G., "Comments on 'Controllability, Stabilizability, and Matrix Riccati Equations for Periodic Systems' and on 'On Solution of Periodic Riccati Equations,'" *IEEE Transactions on Automatic Control,* Vol. AC-32, No. 3, 1987, pp. 270,271.

[15]Bittani, S., Bolzern, P., Colaneri, P., and Guardabassi, G., "Periodic Solutions of Periodic Riccati Equations," *IEEE Transactions on Automatic Control,* Vol. AC-29, No. 7, 1984, pp. 665–667.

[16]Hindmarsh, A. C., "ODEPACK, A Systematized Collection of ODE Solvers," *Scientific Computing,* Vol. 1, IMACS Transactions on Scientific Computation, edited by R. S. Stapleman et al., North-Holland, Amsterdam, 1983.

[17]Al-Rahmani, H. M., and Franklin, G. F., "A New Optimal Multirate Control of Linear Periodic and Time-Invariant Systems," *IEEE Transactions on Automatic Control,* Vol. 35, No. 4, 1990, pp. 406–415.